Faraday Discussions

Accepted Manuscript

This manuscript will be presented and discussed at a forthcoming Faraday Discussion meeting. All delegates can contribute to the discussion which will be included in the final volume.

Register now to attend! Full details of all upcoming meetings: http://rsc.li/fd-upcoming-meetings

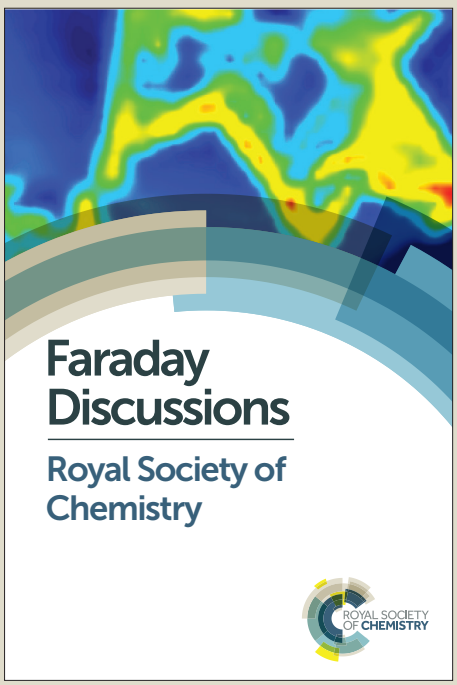

This is an *Accepted Manuscript*, which has been through the Royal Society of Chemistry peer review process and has been accepted for publication.

Accepted Manuscripts are published online shortly after acceptance, before technical editing, formatting and proof reading. Using this free service, authors can make their results available to the community, in citable form, before we publish the edited article. We will replace this *Accepted Manuscript* with the edited and formatted *Advance Article* as soon as it is available.

You can find more information about *Accepted Manuscripts* in the Information for Authors.

Please note that technical editing may introduce minor changes to the text and/or graphics, which may alter content. The journal's standard Terms & Conditions and the Ethical guidelines still apply. In no event shall the Royal Society of Chemistry be held responsible for any errors or omissions in this *Accepted Manuscript* or any consequences arising from the use of any information it contains.

ROYAL SOCIETY OF CHEMISTRY

www.rsc.org/faraday_d

A facile two-step method for fabrication of plate-like WO_3 photoanode under mild conditions

Nan Wang,[a,b] Jian Zhu,[a,b] Xiaojia Zheng, [a,b] Fengqiang Xiong, [a,b] Baokun Huang, [a] Jingying Shi*[a] and Can Li*[a]

DOI: 10.1039/b000000x [DO NOT ALTER/DELETE THIS TEXT]

Fabrication of photoelectrode at large-scale, low-cost and high efficiency is a challenge for practical application in photoelectrochemical (PEC) water splitting. In this work, a typical plate-like WO_3 photoanode was fabricated with chemical etching of the as-prepared mixed metal W-M-O (M = Cu, Zn or Al) oxides by a reactive magnetron co-sputtering technique, which results in a greatly enhanced PEC performance for water oxidation in comparison with that obtained from a conventional magnetron sputtering method. The current approach is applicable for the fabrication of some other semiconductor photoelectrodes and is promising for scaling up application for highly efficient solar energy conversion systems.

1 Introduction

Photoelectrochemical (PEC) water splitting has been regarded as a promising way to produce hydrogen from water and solar energy.[1-3] Photoelectrode, a conductive substrate supported semiconductor thin film material in general, is the crucial part of a photoelectrolysis cell. Depending on the techniques and preparation conditions, photoelectrodes may present different structural, optical and electrical behaviors, and consequently different PEC performance.

Reactive magnetron sputtering technique has been widely used in industry for preparing large area and uniform films well connected to the substrates. The structure of the deposited film can be easily controlled by adjusting the process parameters, and it is also quite easy to repeat the producing process. Hence, this technique shows huge potential for practical large-scale manufacturing of thin film materials. Some metal oxide or oxynitride photoelectrodes such as TiO_2[4], WO_3[5], $BiVO_4$[6] and TaON[7] had been prepared by this method for PEC water splitting, which showed good stability and anti-corrosion properties in electrolyte. However, these films generally present mirror-like surface as well as compact structure that result in high reflectivity and small contact surface area with electrolyte, which make their PEC water splitting performances greatly limited. To overcome this shortcoming, we intentionally introduce other metal oxide through magnetron co-sputtering and subsequently remove the impurity phase by chemical etching to fabricate porous photoelectrodes with higher PEC activity.

WO_3 is a well-known semiconductor material for photoanode as it can absorb part of visible light and shows a remarkable stability in acidic solutions.[8, 9] Porous WO_3 photoanodes can be fabricated generally through liquid-phase routes. For example, Amal et al.[10] prepared flower-like nanostructured tungsten oxide hydrate thin films by electrochemical anodization of tungsten foil at high potentials. Widenkvist et al.[11] obtained the plate-like $WO_3 \cdot H_2O$ films on tungsten substrate in acid media at temperatures higher than 50 °C. While Yang and Demir's groups synthesized the

tungsten trioxide hydrate ($WO_3 \cdot 1/3H_2O$) films via conventional hydrothermal technology at higher than 120 °C [12, 13]. Recently our group successfully fabricated the hexagonal nanoflower $WO_3 \cdot 1/3H_2O$ array on fluorine-doped tin oxide (FTO) substrates by microwave-assisted hydrothermal method.[14] All above as-prepared WO_3 hydrate ($WO_3 \cdot nH_2O$) thin films can convert into WO_3 phase via calcination at about 450 °C without changing morphology. In other words, nanocrystalline WO_3 films prepared by these liquid-phase synthesis methods possess porous network structures, and often exhibit a large surface area as well as enhanced light absorbance. However, these wet chemical synthesis routes usually need high reaction temperatures or high anodization voltages which are difficult to operate in large scale.

In this work, some impurity metals (M = Cu, Zn or Al) were sputtered together with tungsten to produce the mixed W-M-O compounds thin films on FTO glass substrates. After soaking in acid solution of HCl, H_2SO_4 or HNO_3 for etching at room temperature, these extra metal oxides disappeared due to dissolution in acidic media while a porous plate-like WO_3 phase, distinct from those conventional compact WO_3 thin films prepared by a magnetron sputtering, were left behind with twice photocurrent enhancement for PEC water oxidation. This approach can be general and useful for the fabrication of some other semiconductor photoelectrodes.

2 Experimental

Sample preparation

Samples of W-M-O films (M could be Cu, Al or Zn) were deposited on the commercial FTO (NSG, sheet resistance of 20 Ω per square) glass substrates by reactive magnetron co-sputtering system (PVD75 Kurt J. Lesker Company). The FTO glass substrates were cleaned in acetone/isopropanol/ethanol/DI water in sequence. The co-sputtering system consists of two DC guns, loaded with a 99.95% pure W target and 99.99% pure Cu (or 99.99% pure Zn, 99.99% pure Al) target, respectively. The target-substrate distance was fixed at 170 mm. Both targets have a diameter of 3 inches and thickness of 3 mm. After pressure pumped down to 7×10^{-7} torr, the O_2 and Ar gases (99.99% purities) were introduced into the chamber through the mass flow controllers and the gas flow was set for an $[O_2]/([Ar]+[O_2])$ ratio of 38%. The oxygen partial pressure and the total sputtering pressure were 2 and 10 mtorr, respectively. The sputtering power of tungsten target was fixed at about 150 W while the M content in the films was controlled by varying the sputtering power applied to M target. The sputtering power was 60, 60 and 70 W for Zn, Al and Cu targets, respectively. The as-sputtered samples were immersed in an aqueous solution of H_2SO_4, HNO_3 or HCl for various periods of time. Subsequently, the as-etched photoelectrodes were washed with deionized water and followed by calcination in air at 500 ^{o} C for 2 h.

Characterization

The crystal structure was measured by X-ray powder diffraction (XRD, Rigaku D/Max-2500/PC powder diffractometer) using Cu Kα (λ = 0.15406 nm) radiation with an operating voltage of 40 kV and an operating current of 200 mA. The scan rate is 5 ^{o}/ min in the range of 10 ^{o} – 60 ^{o}. Surface morphology and dopant concentration were measured with scanning electron microscopy (SEM, Quanta 200 FEG). Surface profile was used to characterize the film thickness and the roughness (Dektak 150 Surface Profiler, Veeco). Optical properties were measured using Agilen Cary 5000 UV-vis spectrophotometer. Raman spectra were collected using Renishaw inVia Raman spectrometer excited by a

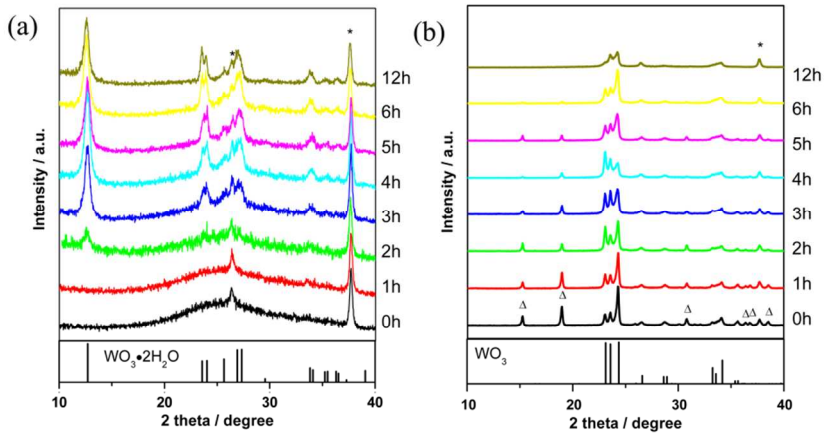

Fig. 1 (a) XRD patterns for the as-sputtered samples etching in 1 M H_2SO_4 aqueous solution for varied periods. (b) XRD patterns of etched W-Cu-O samples after calcination in air at 500 ^oC for 2h. The peaks marked with Δ are assigned to $CuWO_4$ and the peaks marked with * to FTO substrate.

solid laser (532 nm), and the spectra resolution is 1.5-2 cm^{-1}. In order to investigate the chemical bonding and dopant concentration, X-ray photoelectron spectroscopy (XPS) were recorded on a KROTOS AMICAS spectrometer (Shimadzu, Japan) with a magnesium Kα X-ray source. The carbon C1s line with position at 284.8 eV was used as a reference to correct the charging effect. The as-sputtered W-Zn-O, W-Cu-O films and the samples after etching in 1M H_2SO_4 for 12 h were washed in 1M KOH solution (10mL). The size of each electrode was fixed at 15 mm × 20 mm and the thickness was about 1 μm. W, Cu and Zn concentrations of leached solutions were analyzed by inductively coupled plasma atomic emission spectrometry (ICP-AES) on Shimadzu ICPS-8100.

Photoelectrochemical measurement

The photoelectrochemical properties were measured by a CHI electrochemical analyser (CHI 440B, CH Instruments, Inc.). Chopped I-V curves of the as-prepared thin films were performed under simulated AM 1.5 solar illumination (100 $mW \cdot cm^{-2}$) using three electrode setup which the as-prepared samples as working electrode, platinum foil as counter electrode, saturated calomel electrode (SCE) as reference electrode in 0.5 M Na_2SO_4 (pH 3.0) with scan rate of 20 mV/s. Electrochemical impedance spectra (EIS) was measured with frequency range of 100 kHz - 100 mHz and AC amplitude of 10 mV using an electrochemical workstation (IM6 Zahner, Germany). Relative electrochemical surface area (ECSA) was determined from capacitance measurements carried out in the dark by cyclic voltammetry in the region between 0.15 and 0.35 V vs. SCE in 0.5 M Na_2SO_4 (pH 3.0), and the scan rates were varied between 25 and 300 mV/s.

3 Results and Discussion

Figure 1a exhibits the XRD patterns for the as-sputtered samples etching in 1 M H_2SO_4 aqueous solution at different time intervals. Besides the characteristic diffraction peaks represent for FTO substrate, a broad peak in the range of 15-35 ^{o} certainly indicates an amorphous phase for the as-sputtered film. Hardly any new phase can be detected when the sample was etched for only 1 h. While a new diffraction peak located at about 12.7 ^{o}

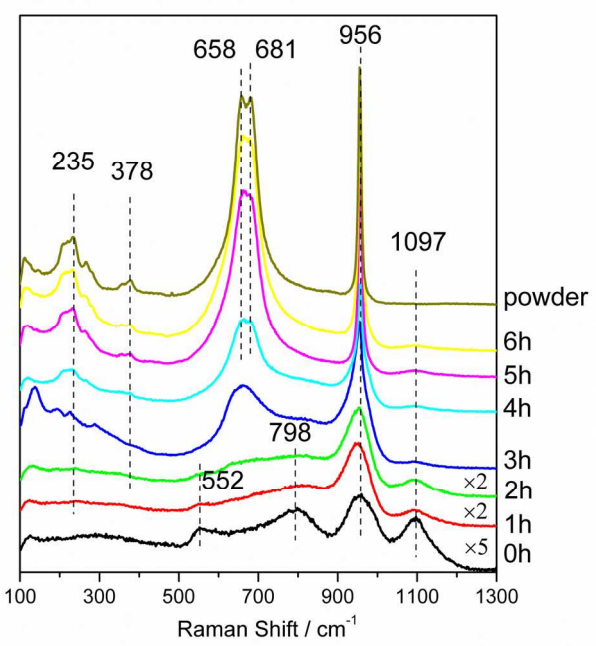

Fig. 2 Raman spectra of samples prepared at different etching times and the precipitation in the solutions.

appears after soaking for 2 h. Extending the etching time to 3 - 12 h, the diffraction peaks corresponding to $WO_3 \cdot 2H_2O$ (JCPDS card No. 18-1420, monoclinic, P2/m(10)) can be clearly observed. The increased diffraction intensity and narrowed full width at half-maximum (FWHM) of the characteristic peaks with etching time suggest an improved crystallinity and a larger grain size. After calcined at 500 ^{o} C for 2 h, the XRD patterns for the corresponding samples are shown in Figure 1b. Clearly, the mixed crystallized phases of WO_3 and $CuWO_4$ (JCPDS card no. 43-1035 and no. 72-0616) are presented when the etching time was shorter than 5 h, while a pure monoclinic WO_3 phase can be achieved after the as-sputtered sample was further corroded for 6 h or more time. These results may suggest that the residual copper can react with tungsten oxide to produce $CuWO_4$ in calcination process and the impurity copper can be completely removed by etching.

The phase transformation in the surface region was further investigated by Raman spectroscopy (in Figure 2). Compared with the Raman spectroscopy of the blank FTO substrate (Figure S1), the bands at 552 cm^{-1} and 1097 cm^{-1} are originated from the FTO substrate so that those at 798 cm^{-1} and 956 cm^{-1} should be assigned to W-Cu-O compound for the as-sputtered sample, which is also different from the Raman bands for the as-sputtered tungsten oxide (Figure S1). This result obviously indicates the successful introduction of impurity copper by co-sputtering. The signals from the substrate as well as the intensity of the band at 798 cm^{-1} become weak when the etching time was in 2 h. However, the Raman scattering at 956 cm^{-1}, which is originated from the symmetric stretching mode of terminal W=O bond, stays the same intensity. Extending the etching time to 3 h, the band at about 645 cm^{-1} appears, indicating that the oxide is converted into $WO_3 \cdot H_2O$ gradually.[15] This broad band is blue-shifted to 670 cm^{-1} which is assignable to the stretching mode of the

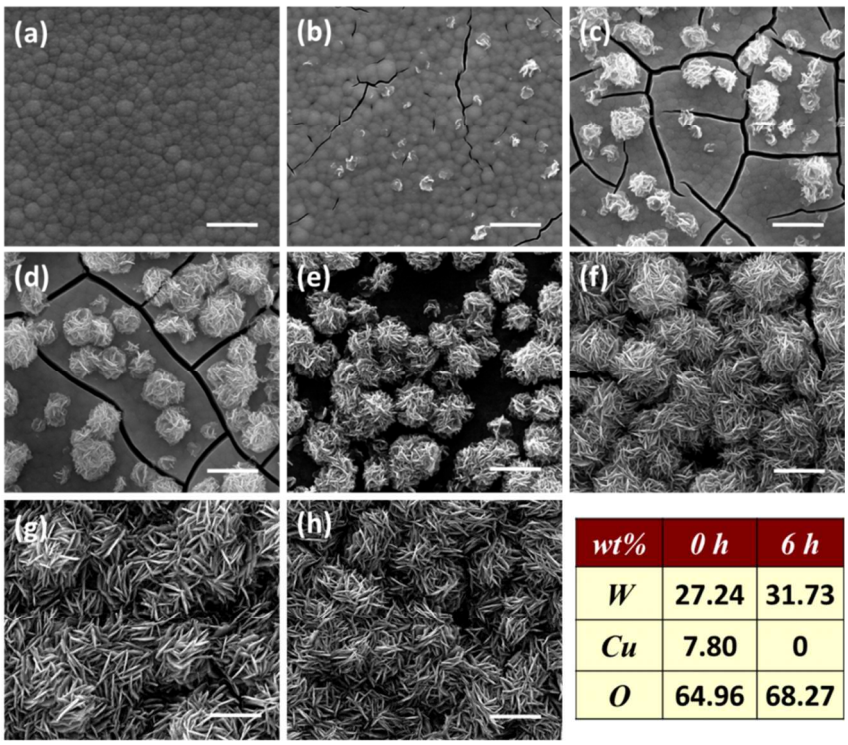

wt%	0 h	6 h
W	27.24	31.73
Cu	7.80	0
O	64.96	68.27

Fig. 3 SEM images of amorphous W-Cu-O films with different chemical etching duration to investigate the growth of plate-like structure. (a) 0 h, (b) 1 h, (c) 2 h, (d) 3 h, (e) 4 h, (f) 5 h, (g) 6 h, (h) 48 h and EDX elemental analysis. Scale bar: 1 μm

W-O-W bonds, gaining higher intensity with increasing etching time to 4 h. As the time was prolonged to 5 h, this band splits into two bands at 658 and 681 cm^{-1}, respectively, which may indicate the $WO_3 \cdot H_2O$ phase had evolved into $WO_3 \cdot 2H_2O$. Besides, the signal from the W=O bond at 956 cm^{-1} is greatly enhanced. On the other hand, the lower frequency bands at 378 cm^{-1} (W-OH_2 vibration) and 235 cm^{-1} (W-O-W bending vibration) appear. These bands are significantly influenced by the degree of hydration and can be used as a spectral marker to determine the hydration level of WO_3.[15, 16] The yellowish precipitate present in the etching solution was also collected for Raman measurement and it shows a doublet narrow bands at 658 and 681 cm^{-1} corresponding to $WO_3 \cdot 2H_2O$.

The surface morphologies observed by SEM at different chemical etching time intervals are illustrated in Figure 3. The as-sputtered sample shows compact morphology (Figure 3a) which is similar to those film materials deposited by single magnetron sputtering technique.[5, 17] After one hour's etching, small pinholes and cracks appear at random, together with some platelets present on the surface as shown in Figure 3b. When the etching time was increased to 2 h, the number of cracks and the width of gaps are developed. The platelets aggregated to form spheroidal structures (Figure 3c). Further extension of etching time, these spheroidal structures become larger until they cover up the whole surface with diameter of about 1 μm and the thickness of each platelet is about

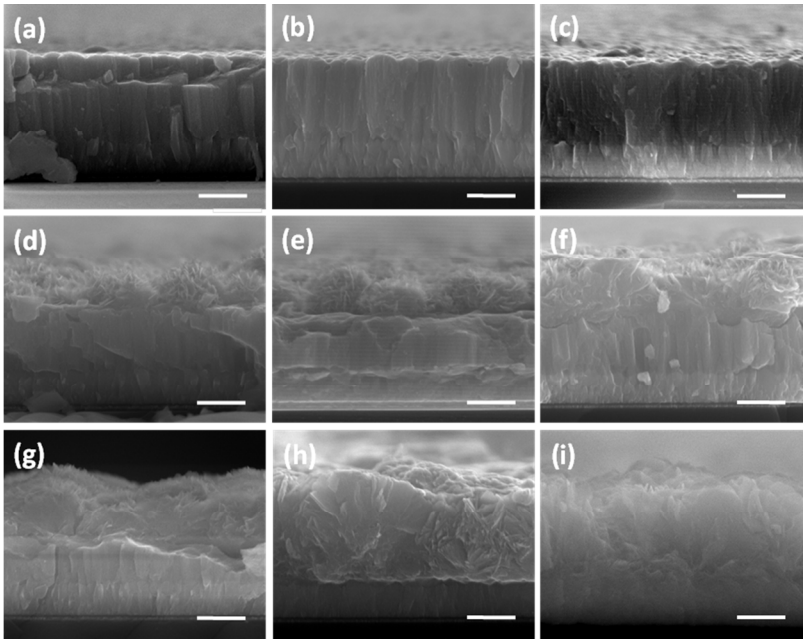

Fig. 4 Cross-section SEM images of amorphous W-Cu-O films after different chemical etching duration. (a) 0 h, (b) 1 h, (c) 2 h, (d) 3 h, (e) 4 h, (f) 5 h, (g) 6 h, (h) 12 h and (i) 48 h. Scale bar: 500nm

80 nm, while pores and cracks vanish gradually when the etching time is extended to 5 h (Figure 3d-f). The plate-like morphology and particle size keep almost unchanged even after a longer time's etching up to 48 h (Figure 3g-h). The element atom ratios detected by EDX analysis are listed in the inserted table, and it can be seen that W element remains while the content of Cu decreases to the detection limit after etching for 6 h. The cross sectional SEM images for samples in Figure 3 were also detected with the results shown in Figure 4. It is observed that the platelets appear on the surface and then permeate to the bulk of film gradually without significant change of the film thickness, which implies that the dissolution and crystallization are processed simultaneously.

For comparison, the as-sputtered tungsten oxide film was also immersed into the acid solution for several hours. The compact film seems to be marginally dissolved after 6 h treatment via SEM observation in Figure S2, showing much slower reaction rate than the amorphous W-M-O films etched in acid solution presented in Fig 3, S3 and S4, which means the presence of impurity metal can accelerate the corrosion process.

The chemical surface states of the as-sputtered W-Cu-O films before and after etching were characterized by X-ray photoelectron spectroscopy (XPS) as shown in Figure 5. Before etching, the two main peaks of Cu 2p located at 932.0 and 951.9 eV correspond to the Cu $2p_{3/2}$ and Cu $2p_{1/2}$, and the satellites peaks on the high energy side are clearly observed. After etching, there are no Cu signals detected (in Figure 5a). Spectra of W4f peaks presented in Figure 5b are dominated by a spin-orbit doublet at binding energies of 37.85 eV ($W4f_{5/2}$) and 35.70 eV ($W4f_{7/2}$), which are associated with the W^{6+} oxidation state. The O 1s spectra of the as-prepared sample shows a peak located at 530.7 eV in Figure 5c, which corresponds to W=O bonding modes. And a small peak appears in region 533.1 eV after etching, which is also the signal from H_2O molecules bound in WO_3.[15]

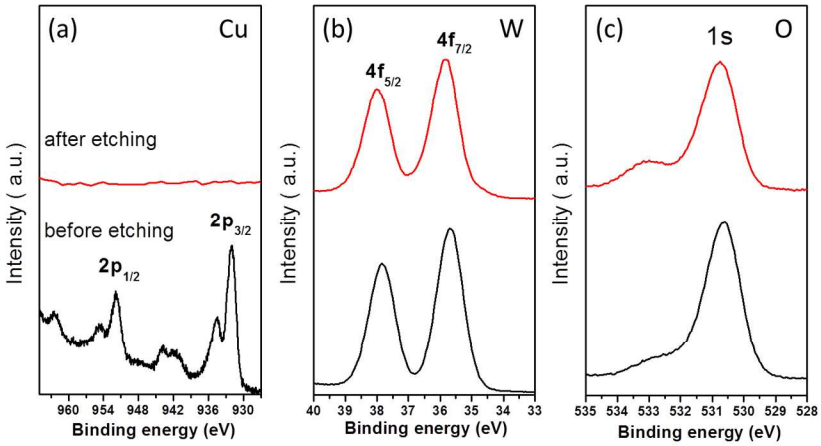

Fig. 5 XPS spectra of the as-sputtered film before and after etching. (a) Cu 2p, (b) W 4f and (c) O1s.

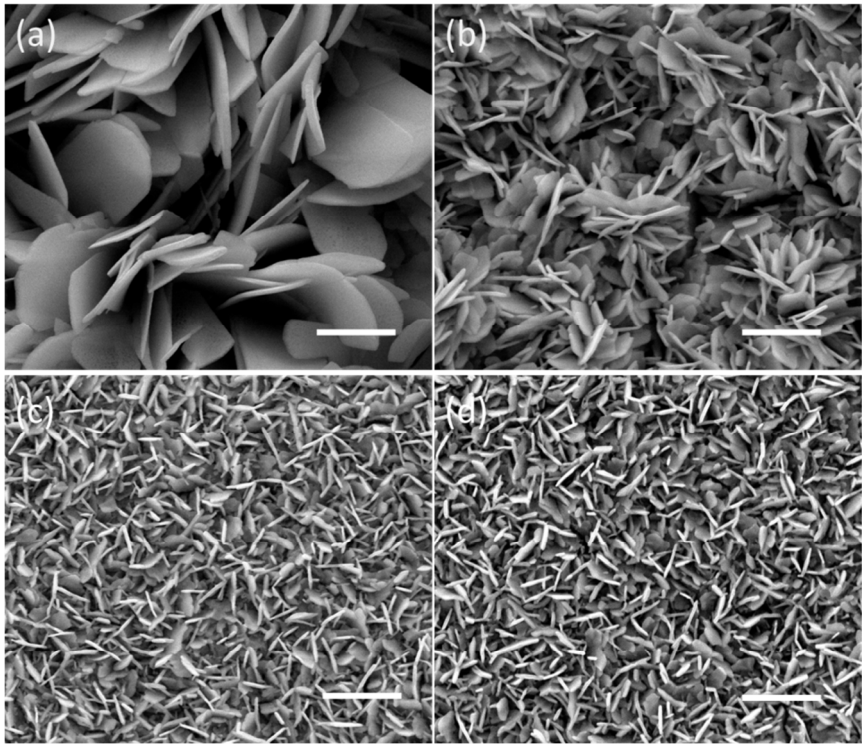

Fig. 6 SEM images of W-Cu-O film etched in (a) 0.5M HCl, (b) 1M HCl, (c) 2M HCl (d) 4M HCl at room temperature; scale bars: 1 μm

Instead of copper, aluminum and zinc were also used as the impurity metal sources for reactive magnetron co-sputtering to deposit W-Al-O and W-Zn-O mixed oxide films on FTO substrates. During the chemical etching process in acidic solution, similar morphology evolutions are observed from the compact surface to pinholes and cracks to

a final plate-like crystals aggregated structure (as shown in Figure S2, S3). Further SEM studies investigated the influence of acid concentration on the shape and size variation, as shown in Figure 6. It reveals that the quantity of acid plays an important role in determining the final morphology of the electrode. In 0.5 M HCl aqueous solution, some large plate structures are obtained (Figure 6a). Increasing the concentration of HCl to 1.0 M, there are middle-size agglomerated plates on the surface (Figure 6b). It is also observed that the aggregations of the plates with smaller size are obtained when further increasing the concentration of HCl (Figure 6c-d), which demonstrate that the number of formed nuclei increase as well as the size of particles decreases. The difference of shape can be explained in the form of the different growth rates of different crystal faces.[18] The SEM images of the obtained photoanodes prepared by different impurity metal under the same acid solution concentration in the etching process are compared in Figure S5, which reveals almost the same size and thickness with similar plate-like morphologies. These results indicate that this method is a general approach toward the fabrication of plate-like tungsten oxide hydrate. Comparing to conventional hydrothermal synthesis or anodizing approaches, the etching method is effective and operative at ambient temperature and atmospheric pressure.

In order to verify the purity of product, the compositions of the as-sputtered sample and etched sample (12 h) were further detected via ICP-AES analysis. The Cu/W molar ratio of W-Cu-O film decreasing from 32.65% to 0.3%, and similarly the Zn/W molar ratio of W-Zn-O film decreasing from 17.72% to 0.03% (as listed in Table S1), which confirms the removal of the impurity metal sources as indicated in above.

Based on the above experimental results, we propose that growth of $WO_3 \cdot 2H_2O$ crystal follows the dissolution-recrystallization mechanism during chemical etching at room temperature, which can be described by following reactions:

$$\text{W-M-O} + (n+2)\ H^+ \rightarrow WO_2^{2+} + M^{n+} + H_2O \ (\text{M = Cu, Al, Zn; n = 2 or 3}) \quad (1)$$

$$WO_2^{2+} + 2H_2O \rightarrow WO_3 \cdot H_2O + 2H^+ \quad (2)$$

$$WO_3 \cdot H_2O + H_2O \rightarrow WO_3 \cdot 2H_2O \quad (3)$$

When soaking into the strong acidic aqueous solution, the as-sputtered amorphous W-M-O film was gradually dissolved and tungsten element exist in the form of WO_2^{2+} (as have been reported[19, 20]) and M^{n+} cations through corrosive pitting. The released WO_2^{2+} species quickly bond with the surrounding water molecules to form insoluble $WO_3 \cdot H_2O$ nucleus while M^{n+} cations spread into the solution resulting in the leaching of impurity metal oxide. As etching time goes on, WO_2^{2+} and M^{n+} cations are continuously produced so that the grain size of $WO_3 \cdot H_2O$ crystals become increasingly larger and the M^{n+} cations simultaneously dissolve into the solution, leading to a final pure phase of tungsten oxide hydrate deposited on the surface. Certainly, it is reasonable for the $WO_3 \cdot H_2O$ to further bond with another H_2O molecule to convert into $WO_3 \cdot 2H_2O$ completely, as indicated by the above Raman analysis. A scheme for the formation mechanism of plate-like tungsten oxide hydrate ($WO_3 \cdot 2H_2O$) is shown in Figure 7. In addition, it is noticed that the crystal size of the obtained $WO_3 \cdot 2H_2O$ increases with more dilute acidic solution as etching media, as observed above in Figure 6. This is because the amount of WO_2^{2+} ions initially produced is smaller in a dilute acidic media than that obtain in a dense one, implying a smaller quantity of nucleation centers and a larger crystal size as a result. This phenomenon further confirms the above dissolution-recrystallization mechanism.

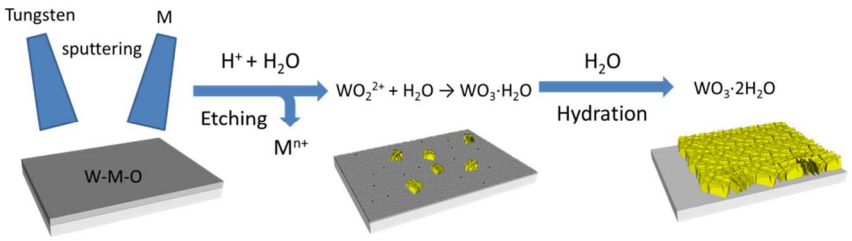

Fig. 7 Scheme for the formation mechanism of plate-like tungsten oxide hydrate ($WO_3 \cdot 2H_2O$)

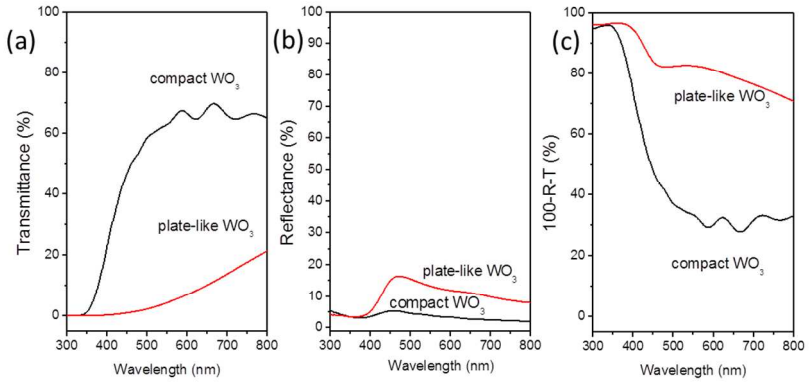

Fig. 8 UV-Vis spectra of compact WO_3 (dash) and plate-like (solid) WO_3 films grown on FTO substrate. (a) transmittance, (b) reflectance and (c) absorption (100-R-T) spectra of the prepared photoelectrodes.

Figure 8 compares the optical properties of the plate-like WO_3 film prepared by the current two-step method (Cu as impurity source and etched in 1 M H_2SO_4 for 12 h) and the compact WO_3 deposited via the conventional magnetron sputtering technology, both thickness of which are controlled to be ~1 μm. It is seen from Figure 8a that the optical transmittance for the plate-like films is under 20% in the visible light range, which is much lower than that of the compact one (~ 60%). The surface roughness estimated from the reflectance property (Figure 8b) by profiler is 6.9 and 68.6 nm for compact and plate-like WO_3 films, respectively (shown in Figure S6), indicating an effective surface roughening by etching treatment. Despite of the higher light reflectance as shown in Figure 8b, the porous WO_3 still has much higher light absorption ability than the compact one (shown in Figure 8c, evaluated according to the formula: A = 100 - R - T), which can be attributed to increased absorption paths among plate-like structures.

The morphological changing not only affects the roughness but also the surface area, which could play a major role in reaction activity. The relative electrochemical surface areas (ECSA) of electrodes are determined from the capacitive region of cyclic voltammograms, as shown in Figure 9. The measurements were carried out in the region between 0.15 and 0.35 V vs SCE in 0.5 M Na_2SO_4 (pH 3.0) in dark. Figure 9a shows the capacitive current for plate-like WO_3 film at six different scan rates from 25 to 300 mV/s, while C-V curves of compact WO_3 and plate-like WO_3 photoanodes (scan rate = 50 mV/s) are compared in Figure 9b. The linear relationships between the capacitive current and scan rate for the two electrodes are plotted in Figure 9c. Assuming that the intrinsic

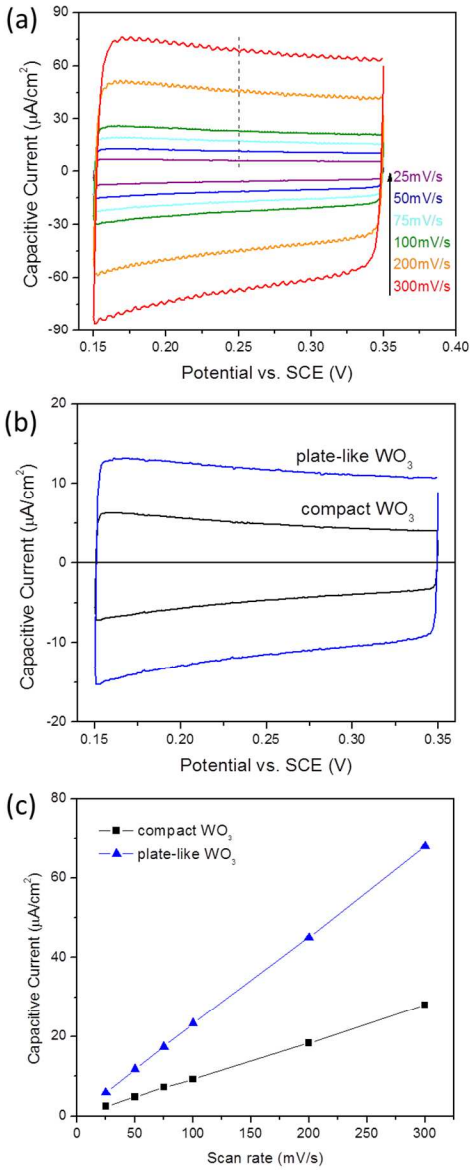

Fig. 9 (a) Cyclic voltammograms of plate-like WO_3 electrode tested at different scan rates. (b) C-V curves of compact WO_3 and plate-like WO_3 electrodes (scan rate = 50 mV/s). (c) The linear relationship between the capacitive current and scan rate.

specific surface capacitance of all the films is approximately the same, the relative surface area of the films can be determined.[21] The relative electrochemically active surface area of plate-like WO_3 is twice as large as sputtered compact WO_3 film.

Photoelectrochemical behavior of the plate-like and compact WO_3 photoanodes was measured by chopped light linear sweep voltammogram in 0.5 M Na_2SO_4 solution (pH 3.0) and compared in Figure 10a. Clearly, the plate-like WO_3 electrode shows higher saturation photocurrent density than the compact one although nearly the same onset

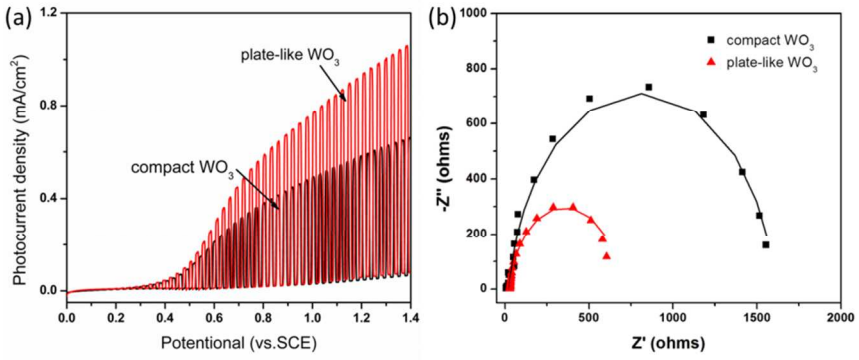

Fig. 10 (a) Linear sweep voltammetric scans of compact and plate-like WO_3 photoanodes in 0.5 M Na_2SO_4 (pH 3.0) under chopped AM 1.5G illumination; Scanning rate: 20 mV/s. (b) Electrochemical impedance spectra and Nyquist plots of the compact and plate-like WO_3 photoanodes measured at 1.0 V vs. SCE in 0.5M Na_2SO_4 solution (pH 3.0) under AM 1.5G illumination.

potential as about 0.2 V vs. SCE is found for the two photoanodes. At the bias of 1.2 V vs. SCE, the photocurrent density generated over the porous sample is 0.95 mA/cm^2, which is almost twice of that generated over the compact one (0.58 mA/cm^2). In addition, the PEC performance of the samples prepared at different etching intervals following a calcination in air at 500 ^{o}C were also measured as shown in Figure S7. The photocurrent of the electrodes decrease with the shortening of the etching time and the as-sputtered W-Cu-O electrode without etching has the lowest photocurrent density, which reveals that the existence of Cu should be harmful to the PEC water oxidation reaction. After complete removal of the impurity metal, the saturation photocurrent density for the sample is 5 folds as high as that of un-etching one.

Electrochemical Impedance Spectroscopy (EIS) was used to gain more insight into reasons for the high photocurrent of the plate-like photoanode. EIS of compact WO_3 and plate-like WO_3 photoelectrodes were measured under irradiation by AM 1.5G light (100 mW·cm^{-2}), with bias voltage of 1.0 V vs. SCE, are shown in Figure 10b. The semicircle for compact WO_3 is larger than plate-like WO_3 sample, indicating that the latter one has lower charge-transfer resistance. The fitted values of solution resistance (Rs), charge transfer resistance across the interface (Rp) and constant phase elements (CPE-T and CPE-P) were calculated and listed in Table S2. The fitted values of Rp are 1576 Ω and 655.5 Ω for the compact WO_3 and plate-like WO_3 samples, respectively, implying the plate-like structure is beneficial for this charge transfer process.

Based on the above analysis, the improvement in the PEC water oxidation activity for the porous plate-like WO_3 photoanode can be mainly attributed to the increase of exposed surface area, light absorption and lower electrode/electrolyte interface charge transfer resistance.

4 Conclusions

In this work, porous plate-like tungsten oxide photoelectrode is successfully prepared on FTO substrate by a facile two-step route concluding magnetron co-sputtering and chemical etching methods. The process of growth includes the dissolution of the as-sputtered amorphous W-M-O films in acidic medium, species precipitation and recrystallization process. Compared to the compact WO_3 film counterparts, the photocurrent of PEC water oxidation with plate-like WO_3 photoanode is improved

significantly because the porous structure provides more exposed surface area, light absorption and lower electrode/electrolyte interface charge transfer resistance.

Acknowledgements

This work was financially supported by the National Natural Science Foundation of China (No. 21090340) and 973 National Basic Research Program of the Ministry of Science and Technology (No.2014CB239400).

References

[a] *State Key Laboratory of Catalysis, Dalian Institute of Chemical Physics, Dalian National Laboratory for Clean Energy, Chinese Academy of Sciences, 457 Zhongshan Road, Dalian 116023, China. Fax: +86 411 84694447; Tel: +86 411 84379070; E-mail: canli@dicp.ac.cn; jingyingshi@dicp.ac.cn*
[b] *University of Chinese Academy of Sciences, Beijing, 100049, China.*
† Electronic Supplementary Information (ESI) available: [Raman spectra, SEM images, linear sweep voltammetric scans curves and tables]. See DOI: 10.1039/b000000x/

1. M. G. Walter, E. L. Warren, J. R. McKone, S. W. Boettcher, Q. X. Mi, E. A. Santori and N. S. Lewis, *Chem Rev*, 2010, **110**, 6446-6473.
2. B. D. Alexander, P. J. Kulesza, I. Rutkowska, R. Solarska and J. Augustynski, *Journal of Materials Chemistry*, 2008, **18**, 2298.
3. H. M. Chen, C. K. Chen, R. S. Liu, L. Zhang, J. Zhang and D. P. Wilkinson, *Chemical Society reviews*, 2012, **41**, 5654-5671.
4. H. Kikuchi, M. Kitano, M. Takeuchi, M. Matsuoka, M. Anpo and P. V. Kamat, *J Phys Chem B*, 2006, **110**, 5537-5541.
5. B. Marsen, E. L. Miller, D. Paluselli and R. E. Rocheleau, *International Journal of Hydrogen Energy*, 2007, **32**, 3110-3115.
6. L. Chen, E. Alarcón-Lladó, M. Hettick, I. D. Sharp, Y. Lin, A. Javey and J. W. Ager, *The Journal of Physical Chemistry C*, 2013, **117**, 21635-21642.
7. D. Yokoyama, H. Hashiguchi, K. Maeda, T. Minegishi, T. Takata, R. Abe, J. Kubota and K. Domen, *Thin Solid Films*, 2011, **519**, 2087-2092.
8. X. Liu, F. Wang and Q. Wang, *Physical chemistry chemical physics : PCCP*, 2012, **14**, 7894-7911.
9. C. Santato, M. Odziemkowski, M. Ulmann and J. Augustynski, *Journal of the American Chemical Society*, 2001, **123**, 10639-10649.
10. C. Ng, C. Ye, Y. H. Ng and R. Amal, *Crystal Growth & Design*, 2010, **10**, 3794-3801.
11. E. Widenkvist, R. A. Quinlan, B. C. Holloway, H. Grennberg and U. Jansson, *Crystal Growth and Design*, 2008, **8**, 3750-3753.
12. W. Li, C. Liu, Y. Yang, J. Li, Q. Chen and F. Liu, *Materials Letters*, 2012, **84**, 41-43.
13. Z. Jiao, J. Wang, L. Ke, X. W. Sun and H. V. Demir, *ACS applied materials & interfaces*, 2011, **3**, 229-236.
14. N. Wang, D. Wang, M. Li, J. Shi and C. Li, *Nanoscale*, 2014, **6**, 2061-2066.
15. M. F. Daniel, B. Desbat, J. C. Lassegues, B. Gerand and M. Figlarz, *J Solid State Chem*, 1987, **67**, 235-247.
16. R. S. Lillard, G. S. Kanner and D. P. Butt, *J Electrochem Soc*, 1998, **145**, 2718-2725.
17. V. S. Vidyarthi, M. Hofmann, A. Savan, K. Sliozberg, D. König, R. Beranek, W. Schuhmann and A. Ludwig, *International Journal of Hydrogen Energy*, 2011, **36**, 4724-4731.
18. B. L. Cushing, V. L. Kolesnichenko and C. J. O'Connor, *Chem Rev*, 2004, **104**, 3893-3946.
19. M. S. Elbasiouny, S. A. Hassan and M. M. Hefny, *Corros Sci*, 1980, **20**, 909-917.
20. J. Johnson and C. Wu, *J Electrochem Soc*, 1971, **118**, 1909-1912.
21. B. A. Pinaud, P. C. K. Vesborg and T. F. Jaramillo, *The Journal of Physical Chemistry C*, 2012, **116**, 15918-15924.